What made TFTR supershots super and JET Hot-ion H-modes hot

R.V. Budny[1,a,*] and JET contributors[a]
EUROfusion Consortium, JET, Culham Science Centre, Abingdon, OX14 3DB, UK
[1] *Princeton University, (retired), Princeton, NJ 08540, USA*
(Dated: July 24, 2019)

The supershot plasma regime [1] in the Tokamak Fusion Test Reactor (TFTR) and the Hot-ion H-mode HIHM regime [2] in the Joint European Torus (JET) achieved relatively high ion temperatures and high fusion reaction rates compared with the baseline regimes having lower core energy. In TFTR supershots central ion and electron temperatures obtained high values ($Ti \lesssim 50$ keV and $T_e \lesssim 14$ keV). The JET alpha heating HIHM discharges also had large central values for T_i, T_e, and T_i/T_e. The causes of the high performance have not been fully understood. This paper presents an explanation for the high central temperatures.

We reexamine discharges from the DT experiments dominated by neutral beam (NB) heating. The discharges with highest core temperatures had relatively low electron density and well-conditioned first walls which allowed deep penetration of the NB neutrals. The beam ion - thermal ion was the dominant plasma heating rate in the central region. Thermal ion - electron energy equilibration was the dominant electron heating rate in the center of supershots and was among the dominant heating rates in HIHM discharges The central ion and electron temperatures co-vary for most of the NB heated phase. The profile shapes of the thermal ion energy density $w_{\rm i}$ and the effective thermal ion heating rate $p_{\rm i}$ had similar shapes at least out to the half-radius and the time evolutions of $w_{\rm i}$ and $\int dt\ p_{\rm i}$ increased similarly during the constant NB power phase. Comparable discharges with lower core energy confinement also have energy profiles with shapes similar to the effective heating profiles, suggesting that the NB energy deposition plays a dominant role in the formation of both regimes.

These regimes with NB heating and enhanced core confinement are not considered for fusion reactors since NB heating does not appear practical for them and since the required high density operation implies $T_i \simeq T_e$ However these regimes might be needed in practical reactors to create "smoldering cores".

Keywords: tokamak experiments, TFTR, JET, deuterium - tritium, neutral beam heating, alpha heating, isotopic mass effects, TRANSP

(Some figures may appear in colour only in the online journal)

1. Introduction

Leading proposals for practical fusion energy rely on alpha particle heating of DT fuel. In principal centrally peaked density and temperatures could achieve the desired conditions with minimal total stored energy. The highest rates of DT fusion reactions in tokamaks were achieved with peaked profiles. These were in the TFTR supershot regime [1] and the JET Hot-Ion H-mode HIHM regime [2]. Other regimes, typically with broader profiles achieved considerably lower peak fusion rates. The global fusion gain parameter $Q_{\rm DT}(\equiv P_{\rm DT}/P_{\rm aux}$ with $P_{\rm DT}$ the DT total fusion power and $P_{\rm aux}$ the applied heating power) reached 0.29 in supershots and 0.76 in HIHM. The largest values for the local fusion energy gain computed by TRANSP [3] in the center were approximately 0.9 and 1.2 respectively

The supershots and HIHM discharges had relatively low electron densities and high central values for T_i, T_e, and T_i / T_e. These high core confinement regimes are typically not not considered to be of use in practical fusion energy reactors which are predicted to require high density implying nearly equilibrated T_i and T_e. Also the NB systems are not considered to be practical in a commercial reactor. However, they might be needed during startup to create "smoldering cores". For instance, reactor plasmas might be started in a two stage process with the first stage using

intense central NB heating in a low electron density n_e plasma with a short path length $\int dl\ n_e$ between the NB injector and the plasma center to allow intense NB ion heating. Then when core ratio of alpha heating to NB heating q_{DT} becomes sufficiently large the plasma shape, position, and density could be altered to achieve larger P_{DT}.

Recent reanalysis [4, 5] of the discharges from the DT campaigns was done to study causes of the high temperatures. The original motivation was to assess if alpha heating had been reliably measured, as claimed and what role isotopic mass enhancement played. The results showed that competing electron heating from ion-electron exchange, beam-ion, and Ohmic heating were comparable or larger. Also non-alpha heating effects such as isotopic or fast beam ion enhancements of the thermal ion confinement could have caused the higher T_e and T_i in DT plasma.

References [4, 5] indicated that the dominant cause of high T_i and T_e was wall conditioning, which allowed deep penetration of neutral beam NB ions. This generated high central T_i which in turn generated high central T_e and T_i/T_e. This was seen in the supershot conditioning series described in [6]. The thermal-ion-electron heating rate p_{ie} is the largest electron heating rate in the center of supershots and is typically at least three to four times the peak alpha heating rate $p_{\alpha e}$ with DT.

A schematic of how an isotopic mass enhancement can complicate experimental verification of alpha heating is shown in **figure 1**. The thermal hydrogenic isotopic mass is defined as $< A >_{hyd} \equiv (n_H + 2n_D + 3n_T)/(n_H + n_D + n_T)$. T_i is shown assuming either no enhancement or an enhancement increasing with $< A >_{hyd}$. The thermal-ion-electron heating rate $p_{ie} \propto (T_i - T_e)$ increases with mass enhancement so T_e would be effected. The schematic T_i and T_e with enhancement are similar to the results seen in the center of JET alpha heating HIHM discharges. Figures 13-b) and 14-b) in [4] show the temperatures at two times during rampup. At later times T_i and T_e have less variation with $< A >_{hyd}$. It is not clear if the enhancement remains in seady state conditions or if the discharges in the data base experienced delectarious MHD.

Strong coupling (interconnected parameters) make it very difficult to separate causes. An example is the approximate relation between $< A >_{hyd}$ in the central region and the fraction of tritium beam power:

$$< A >_{hyd} \ \simeq \ f_{NBT} + 2 \tag{1}$$

This is plausible since beam fueling is the dominant hydrogenic species source near the center. Examples of their values are given in table 1. This correlation complicates experimental separation of possible isotopic effects on T_e and T_i from the thermal plasma or the beam injection. Other examples of strongly coupled parameters are the beam ion D/T mix and energy with $< A >_{hyd}$.

This paper extends the reanalysis beyond the central region. In addition to the thermal ion and electron power balances, the toroidal rotation power balance and the electron species balance equations are discussed.

One of the goals of this paper is to show new ways to quantify alpha heating in future DT experiments, such as planned for JET in 2020 and in ITER starting after 2035. It is instructive to reconsider the TFTR along with the JET alpha heating experiments since the plasma regimes and difficulties encountered contrast each other regimes. Understanding both helps generalize to upcoming experiments.

We study discharges produced in the DT experimental campaigns in TFTR (1993-1996) and JET (1997). We focus on discharges without Ion Cyclotron (IC) heating. Most of the TFTR discharges did not have IC heating. Many of the JET discharges did, but we consider only those from the alpha heating campaign [7] which did not. IC heating was used to simulate effects of alpha heating. Neither tokamak had Electron Cyclotron heating.

2. Covariance of central temperatures and stored energy densities

The central values of T_i and T_e covary nearly linearly at least up to the time of peak T_i. In this paper T_i denotes the temperature of the hydrogenic species calculated by TRANSP from the measured temperature of the carbon impurity [8]. The values of T_i are lower than those for the carbon impurity ions especially for the highest values in the core occurring early in the NB phase. Trajectories of the central T_i versus T_e for a selection of TFTR and JET discharges are shown in **figure 2**. Three TFTR discharges from a sequence of five deuterium (DD) discharges [6] with varying degrees of wall conditioning by Li pellet injection into their Ohmically heated phases are shown in **figure 2-a)**. Typically the trajectories show hysteresis with T_e continuing to increase after T_i saturated, and then to

start to decrease along a higher trajectory. This phenomenon is discussed further below.

For analyzing effects of heating and power balance it is more direct to inspect the stored energy densities. Alpha heating, by definition increases stored energy, but not necessarily temperature. Trajectories of the central thermal and electron energy densities w_e vs w_i are shown in **figure 2-d)**. They increase approximately linearly up to the times of maximum w_i after which w_e continued to increase for awhile until the end of the T_i charge-exchange spectroscopy CX data. Trajectories of the central electron energy densities versus n_e are shown in **figure 2-g)**. Relatively small hysteresis effects are seen indicating that the hysteresis in the T_i vs T_e and w_i vs w_e trajectories is due to changing n_e.

Trajectories for four TFTR supershots are shown in **figure 2-b)**. Three of these are from a triplet of comparable discharges [5]. Also the trajectory of the supershot with highest sustained Q_{DT} is shown. Alpha electron heating should increase as alpha particles are accumulated and slow down. This would be expected to increase the slope of T_e unless the loss rates increase to offset $p_{\alpha e}$.

Trajectories for three JET discharges from the alpha heating experiment are shown in **figure 2-c,f,i)**. The discharges shown are the high performance DT 42856 HIHM, the high performance TT 42840 HIHM, and the lower performance TT 43011 which had high wall recycling rates. These show approximately linear increases to the times of maximum T_i. There was considerable variation in the central n_e values in time.

3. Heating and electron fueling rates increase linearly with temperatures and densities

Section 2 presented evidence that the central T_i and T_e are tightly correlated, suggesting that T_i played an important role in high central T_e. In this section evidence from central NB heating and fueling is discussed. These rely on TRANSP analysis for the central NB deposition. The TRANSP runs used a relatively recent excited states ionization model [9] for ionization of NB neutrals based on ADAS cross-sections [10]. Results for beam deposition in the center are close to those from earlier TRANSP deposition models. TRANSP run IDs are listed in table 2.

Figure 3 shows analysis results from the conditioning series discussed in **figure 2-a)**. The log plots of the electron source rates defined in equation (5) are plotted in **figure 3-a)** at two locations, in the center (x=0) and near the edge (x=0.9). The variable x is the natural radial variable used in TRANSP, defined as the square-root of the normalized toroidal magnetic flux. This is approximately the normalized minor radius. A one-to-one correlation of the central n_e and s_e in supershots was reported in [11]. The limiter conditioning reduced the emission rate of hydrogenic species from the large inner limiter. The s_e edge values decreased in the sequence of discharges as the walls became better conditioned. Their central values increased in time and as the discharges became better conditioned. These trends are consistent with the electron densities shown in **figure 3-b)**. The central n_e values continued to increase in time and with wall conditioning, except for sawteeth and (in the case of 76650) with other MHD, until the end of NB at 4.3s, and then decreased precipitously as n_e decreased.

The central beam-thermal ion heating rates are shown in **figure 3-c)**. These increased by more than 100% with conditioning. So did the measured central values for T_i shown in **figure 3-d)**. The central beam-electron heating rates shown in **figure 3-e)** increased during the rampup phase. The central T_e increased in time and with conditioning as shown in **figure 3-f)**. Note also the T_e afterglows shown in that panel and discussed in the previous section which occurred after the NB (and CX data window). Note that the ion heating was about a factor of 10 greater than the electron heating, i.e., **figure 3-c)** vs **figure 3-e)**. Below we show that the thermal ion-electron heating plays an important role in T_e. The triplet supershots showed a very distinctive bump in the time evolution of the central T_e when the P_{NB} was terminated or decreased to a lower level. These bumps were dubbed T_e afterglows and they were speculated to measure $P_{\alpha e}$ but they were seen in both DD and DT (coincident with a sharp negative $\frac{\partial n_e}{\partial t} dn_e$) [5].

Figure 4 shows analysis results for the triplet of supershots discussed in [4]. **Figure 4-a)** shows the evolution of the central values of the electron source rate in equation (5). These trends are consistent with the central electron densities shown in **figure 4-b)** which continued to increase in time until the rampdown of NB starting at 4.3s, and then decreased precipitously.

The central beam-thermal ion heating rates are shown in **figure 4-c)**. These were about 30% higher with DT, as were the central values for T_i in **figure 4-d)**. The central beam-electron heating rates shown in **figure 4-e)** decreased as the density ramped up. The central T_e increased in time and with DT as shown in **figure 4-f)**.

The corresponding plots for three of the JET alpha heating discharges in **figure 5**. Two of the discharges are a DT and TT HIHM and the third (43011) is a less well conditioned TT. This third had been included in the scan discussed in [7] skewing the conclusions about alpha heating. The electron source rates in **figure 5-a)** show the same trends with conditioning as in TFTR shown in **figure 3-a)**, but their magnitude of values at x=0 and x=0.9 are reversed from the ordering in supershots. This is due to the much flatter or even hollow n_e profiles. The evolution of the central values are shown in **figure 5-b**. The central beam heating rates **figure 5-c,-e)** are highest for the DT HIHM. Profiles of these rates for eight discharges from the alpha heating scan at four times are shown in [4].

To summarize, the correlations of the central parameters show a large increases in the central thermal ion and electron heating rates with wall conditioning. However we find relatively small increases when DD was changed to DT.

4. Profiles from the balance equations

The appendix gives the energy and particle balance equations used by TRANSP in the usual analysis mode for discharges with Ohmic, NB, IC, and alpha heating. Abbreviated versions of the first two were discussed in [4, 5]. The definitions of p_i and p_e there are different due to the truncated versions of equations 2 and 4 in that paper. Central values of energy densities versus the heating powers were shown in [4].

Profiles of terms for p_i defined in equation 2 for two TFTR supershots are shown in **figure 6**. The terms for 89402 with a "postlude" phase (late NB phase with sufficient P_nb for CX data) from the triplet are shown at two times, 4.9s near the peak performance and late in the postlude at 5.3s. The terms for 80539 with record Q_DT are shown at peak time. The largest term in the core for p_i is p_bth, and the next is p_bi. p_ie is a significant sink of energy in the core.

In the TFTR analysis p_e tends to become negative near the edge, driven mainly by p_rad. This could be due to the input p_rad profile being too large near the edge or to errors in other data or the TRANSP analysis. Typically in the TRANSP analysis the input profiles for p_rad came from inversion of bolometry emission measurements reduced by $\simeq 20\%$ to correct for the power coming from charge-exchange neutrals instead of radiation. For the JET analysis inverted bolometer profiles were not available. For these reasons we omit radiation from p_e and consider $p_\mathrm{e-norad} \equiv p_\mathrm{e} - p_\mathrm{rad}$. Profiles of $p_\mathrm{e-norad}$ for the two TFTR supershots are shown in **figure 6**. The largest term in the core for $p_\mathrm{e-norad}$ is p_ie. The alpha-electron heating term is relatively small. The radial profiles of $p_\mathrm{e-norad}$ are centrally peaked, but not as peaked as those of p_i. Their profiles are similar to those of T_e and w_e.

The terms for three JET representative discharges from the alpha heating experiment are shown in **figure 7**. The profiles are shown at 14s which was near peak performance and before the occurrence of significant sawtooth crashes or other obvious MHD. The discharges shown are the high performance DT 42856 HIHM, the high performance TT 42840 HIHM, and the lower performance TT 43011 with high wall recycling rates. For the ion heating powers the sum $p_\mathrm{bi} + p_\mathrm{bth}$ dominates. In the core of the HIHM discharges $p_\mathrm{e-norad}$ is dominated by p_be, p_ie, and $p_{\alpha e}$. The alpha electron heating rate $p_{\alpha e}$ did not became larger than the sum of the other two, making it hard to be confident of its actual value.

5. TIME-INTEGRATED BALANCE

Next we discuss profiles from the time-integrated balance equations 2-5. The integrated source terms in left sides of equations 2-5 give the densities w_i, w_e, w_r, and n_e. The goal is to study heuristically the qualitative and connections of their profiles with the power and electron source terms. Profiles at equal time increments are shown in **figures 8 - 10**. What is remarkable is that the shapes of these densities remain qualitatively similar to the shapes of the time-integrated input terms, at least out to the half radius. The time evolutions are also similar during the steady phase of the main P_nb.

5.1 TFTR supershots

Profiles of $w_{\rm i}$ and $\int dt\ p_{\rm i}$ for the TFTR DT supershot 89402 with medium $P_{\rm nb}$ discussed in [4] are shown in **figure 8-a,-e)**. The radial profiles of $\int dt\ p_{\rm i}$ are very centrally peaked, as are the profiles of $w_{\rm i}$ and T_i. These have similar shapes and increase in time within the x $\simeq$ 0.6 spatial region although $\int dt\ p_{\rm i-cond}$ is slightly broader. This shape similarity continued after the NB power was ramped down in the postlude phase. The time evolutions of $w_{\rm i}$ and $\int^t dt\ p_{\rm i}$ are similar during the constant NB power phase, but the values of $w_{\rm i}$ decreased in the postlude phase whereas $\int^t dt\ p_{\rm i}$ continued to increase.

Profiles of $w_{\rm e}$ and $\int^t dt\ p_{\rm e-norad}$ from the time-integrated balance equation 3 have similar shapes, especially in the core region. The radial profiles of $\int^t dt\ p_{\rm e-norad}$ are centrally peaked, but not as much as are the profiles of $w_{\rm i}$ and T_i. Profiles for 89402 are shown in **figure 8-b)** and **figure 8-f)**. As with the $w_{\rm i}$, $\int dt\ p_{\rm i}$ comparisons the profiles of $w_{\rm e}$ and $\int^t dt\ p_{\rm e-norad}$ are similar but $w_{\rm e}$ is steeper than $\int^t dt\ p_{\rm e-norad}$.

In the analysis of the central power balance [4, 5] the central radiation is a small contributor to $p_{\rm e}$.

Profiles for the toroidal rotation energy $w_{\rm r}$ and time-integrated rotating rates $\int dt\ p_{\rm rot}$ are shown in **figures 8-c)** and **figures 8-g)**. These energies are much smaller that the thermal-ion energy $w_{\rm i}$ shown in panels -e) and -f), and the $\int dt\ p_{\rm rot}$ profiles are much lower than $w_{\rm r}$.

Profiles of the electron density and time-integrated source rates are shown in **figures 8-d)** and **figures 8-h)**. The gradients of $n_{\rm e}$ and $\int dt\ p_{\rm e}$ are similar in the core but beyond the mid-radius the gradient of $\int dt\ p_{\rm e}$ becomes positive. The wall-dominated terms in the left-hand side of equation (3) become large, but unfortunately are poorly known, so there is considerable uncertainty about $p_{\rm e}$ in the outer radii.

The corresponding profiles for discharges from the DD wall conditioning series, discussed in [4, 6] are show similar trends though the peak central values are reduced. These show that the well conditioned supershot 76654 and the comparable poorly conditioned discharge 76649 with low core energy confinement have similar correlated profiles. The low core confinement discharge had slightly broader profiles and slightly lower peak values.

5.2 JET

Analysis results from some of the JET alpha heating series discussed in [3–5] are shown in **figure 9** and **figure 10**. The higher performing alpha heating HIHM such as the DT 42856 (not shown) and the TT 42840 are comparable. Compared with TFTR supershots they are broader with lower central peak values. The less-well conditioned and lower performance TT 43011 is shown in **figure 10**. It was qualitatively similar, but with broader profiles and lower peak values compared with the alpha heating HIHM discharges. The $n_{\rm e}$ profiles in JET were flatter than those in TFTR, and were flatter than the $\int dt\ s_{\rm e}$ profiles even in the core, unlike in TFTR supershots.

Similar analysis was performed for some of the JET ELMy H-mode discharges. An example is the DT 42982 with record $\int dt\ P_{\rm DT} = 22$ MJ. Validation of TRANSP analysis of this discharge was discussed in [12]. Analysis gives results similar to **figure 9, 10** during the first two seconds of NB. During the next three seconds of NB the shapes of $w_{\rm i}$ and $\int dt\ p_{\rm i}$ and for $w_{\rm e}$ and $\int dt\ p_{\rm e}$ remained similar, but $w_{\rm i}$ and $w_{\rm e}$ were approximately constant while $\int dt\ p_{\rm i}$ and $\int dt\ p_{\rm e-norad}$ increased. Thus the NB phase of the alpha heating discharges resembled the early rampup phase of the ELMy discharges.

The similar shapes of $w_{\rm i}$ and $\int dt\ p_{\rm i}$, and of $w_{\rm e}$ and $\int dt\ p_{\rm e}$ implies that the sum of the conduction plus convection terms, the last two in Eqs. 3 and 4 also have similar shapes. Thus instead of transport barriers explaining the core confinement, the drive terms are key. This suggests that sharpening $p_{\rm i}$ can sharpen $w_{\rm i}$ for improved performance. In principal NB parameters are accessible actuators.

6. Revision of early alpha heating and isotopic mass conclusions

Quantifying alpha heating was challenged by the need to disentangle the causes of increased T_e. Alpha heating should be highest when the core DT mix was roughly 50:50. A favorable isotopic effect in the thermal plasma confinement

should increase as the core $< A >_{\rm hyd}$ increases from DD to TT. A hypothesis proposed during the TFTR experiments was that T_i/T_e was large in supershots due to a favorable intrinsic isotopic scaling of ion energy confinement in the thermal plasma [13–16]. An isotopic scaling of $T_i \propto < A >_{\rm hyd}^{0.7}$ was reported for TFTR L-mode and IC plasmas [17]. The range of $< A >_{\rm hyd}$ accessed in TFTR was limited due to significant fueling from latent D emitted by the walls. Even though experiments with TT supershots were performed, the largest values for $< A >_{\rm hyd}$ were $\simeq$2.7. Typical DT and TT supershots had $< A >_{\rm hyd}$ below $\simeq$2.5. JET achieved values near 3.0. The early analysis [7] of the JET alpha heating set excluded the hypothesis of an isotopic mass effect partly based on the tritium beam injection into the tritium plasma TT outlier discharge 43011 [5].

7. Summary of new results

The central T_i and T_e increased nearly linearly **figure 2** which strongly suggests that the core beam ion heating played a decisive role in creating the high central temperatures in these discharges. The dominant heating in the core of TFTR supershots and and JET alpha heating HIHM were the $p_{\rm bi}$ and $p_{\rm bth}$ terms. The approximate correlations of the energy density and $\int dt$ profiles are further evidence of the dominant role of beam heating in establishing and maintaining the high core energy confinement conditions. These are interdependent, but the dominant term was the $p_{\rm bi}$ heating.

The decisive increase in the central T_i and T_e with wall conditioning and lowered electron density was correlated with the increased central beam - thermal ion heating rate. The relatively small increase in the central T_i and T_e with the switch from DD to DT is correlated with a small increase in the central beam - thermal ion heating rate. The hypothesis is that this increase was sufficiently amplified by the circular non-linear coupling to cause the observed the increased T_i and T_e. Thus the central T_i and T_e profiles can be controlled by proper choice of wall conditions and the NB beam deposition.

8. Discussion

One difficulty deducing alpha particle heating in these TFTR and JET discharges is that they did not obtain steady state. Not only the alpha particle effects, which have relative long equilibration times, but also even the plasma energy and particle transport were not steady. This was especially true for the highest power discharges.

The DT experiments in TFTR and JET came close to demonstrating alpha heating. Plots of the evolutions of the volume-integrates alpha heating from the record $Q_{\rm DT}$ TFTR supershot and JET HIHM are shown in **figures 11-a)**. The JET prediction shown has increasing uncertainty after the end of the CX data at 13.3s. The spike starting at 13.4 s could be due to unreliable data. The predicted volume and time integrated alpha heating energies are shown in **figures 11-b)**. Parameters are summarized in table 1.

These results apply only to supershots and Hot-Ion H-modes. Other regimes appear to have different mechanisms determining performance. Isotopic mass scaling of DD and DT TFTR L-mode and Reverse Shear has been reported [17] JET ELMy H-mode plasmas have separate processes effecting core [12] and pedestal [18] energy transport coefficients.

9. Conclusions and recommendations

Neutral beam central heating was instrumental in the creation of supershots and Hot-ion H-mode discharges. The NB heating rate in the core was considerably higher for thermal ions than electrons. The ion heating with tritium was higher than with deuterium. Increased central beam-ion heating was a large contributor to the higher temperatures measured in DT. We conclude that the null hypothesis of no alpha heating in TFTR and JET has a large, but difficult to quantify p-value, the probability. However the calculated alpha heating rates appear consistent and plausible with the experimental data.

Future DT experiments are planned for JET in 2019-2020 and in ITER after 2034. Alpha heating and isotopic mass

experiments in JET would benefit from a more comparable set of discharges, especially including ones with TT NB injection. Avoiding sawteeth could improve the reproducibility for comparisons and simplify the modeling. Also this is expected to increase $p_{\alpha e}$ and T_e. Likewise avoiding transient excursions of the NB power waveforms should help, as would long flattop durations. Discharges with the NB power reduced in postlude phases for CX measurements would be helpful increasing $f_{\rm alp}$ and $Q_{\rm DT}$ and the credibility of the modeling. Measurements such as core hydrogenic ion densities, radiation emission, recycling, and impurity densities are needed for accurate analysis. Separating alpha heating effects from isotopic mass effects are important, especially since isotopic mass enhancements of transport could help make DT fusion energy easier.

This work has been carried out within the framework of the EUROfusion Consortium, and has received funding from the Euratom research and training programme 2014-2018 under grant agreement No 633053. The views and opinions expressed herein do not necessarily reflect those of the European Commission. The computer facilities used for this work were supported in part by the US DoE contract No. DE-ACO2-76-09CHO11466. The authors wish to thank M. Gorelenkova, S. Zweben, and the TFTR and TRANSP teams.

*E-mail: budny@princeton.edu

[a]See author list of [19].

Appendix Energy and particle balance

We extend the thermal ion and electron power terms for energy balance used in [4] to include all the terms calculated by TRANSP using the standard analysis of discharges with beam and alpha particle heating. All the discharges in the TFTR and JET experimental campaigns had at least trace amounts of tritium and thus had computed amounts of alpha heating.

The thermal ion power balance terms computed by TRANSP are:

$$p_{\rm i} \equiv p_{\rm bi} + p_{\rm bth} - p_{\rm ie} - p_{\rm cx} + p_{\rm rotf} + p_{\rm rotc} + p_{\rm cmpi} + p_{\alpha i} + p_{\rm iich} = \frac{\partial w_{\rm i}}{\partial t} + p_{\rm i-conv} + p_{\rm i-cond} \tag{2}$$

with $p_{\rm i}$ the effective thermal ion heating rate, $p_{\rm bi}$ the beam ion - thermal ion collisional heating rate, $p_{\rm bth}$ the beam ion contribution to the thermal ion energy density as beam ions thermalized, $p_{\rm ie}$ the thermal ion - electron heating rate, $p_{\rm cx}$ the net charge exchange loss rate, $p_{\rm rotf}$ the toroidal rotation friction heating rate $p_{\rm rotc}$ the toroidal rotation convection heating rate and $p_{\rm cmpi}$ the thermal ion compression work, $p_{\rm iich}$ the thermal ion icrh, $p_{\alpha i}$ the alpha-thermal ion heating rate, $w_{\rm i}$ the thermal ion energy density, $p_{\rm i-conv}$ and $p_{\rm i-cond}$ the conducted and convected thermal ion energy outflows. The $p_{\rm ie}$ term is a significant contributor to the the ion and electron energy balance when $T_i \gg T_e$, which was especially true in the case of TFTR supershots. The last four terms on the left-hand-side were relatively small for the discharges considered here.

The $p_{\rm bi}$ and $p_{\rm bth}$ terms were combined in [4]. Also small terms were dropped in that publication. The choice of which power terms to consider as sources or sinks is somewhat arbitrary. Here we place the conduction and convection energy flows on the right-hand-side. Since we do not have well verified models for the conduction we consider it as a variable which can be calculated from the balance equations.

The electron power terms for balance are:

$$p_{\rm e} \equiv p_{\rm be} + p_{\rm ie} + p_{\rm oh} - p_{\rm rad} + p_{\alpha e} - p_{\rm ionz} + p_{\rm cmpe} + p_{\rm eich} = \frac{\partial w_{\rm e}}{\partial t} + p_{\rm e-conv} + p_{\rm e-cond} \tag{3}$$

with $p_{\rm e}$ the effective electron energy heating rate, $p_{\rm be}$ the beam ion - electron heating rate, $p_{\rm oh}$ the Ohmic heating rate, $p_{\rm rad}$ the radiation emission rate, $p_{\alpha e}$ the alpha-electron heating, $p_{\rm ionz}$ the ionization work, $p_{\rm cmpe}$ the electron compression work. $p_{\rm eich}$ the IC electron heating, $w_{\rm e}$ the electron energy density, $p_{\rm e-conv}$ and $p_{\rm e-cond}$ the conducted and convected electron energy outflows, The $p_{\rm ie}$ term is the same appearing in equation (2) with opposite sign. The last three terms on the left-hand-side were relatively very small.

Sheared rotation can play an important role in suppressing turbulence. The thermal ion rotation power balance terms are:

$$p_{\rm r} \equiv p_{\rm rbco} + p_{\rm rbth} + p_{\rm rjxb} - p_{\rm rnet} - p_{\rm rfrc} + p_{\rm rcmp} + p_{\rm ntv} + p_{\rm rpl} = \frac{\partial w_{\rm r}}{\partial t} + p_{\rm r-cond} + p_{\rm r-conv} \tag{4}$$

with $p_{\rm r}$ the effective thermal rotation power, $p_{\rm rbco}$ the beam ion - thermal ion collision torque, $p_{\rm rbth}$ the beam ion - thermalization torque added to the thermal ion species, $p_{\rm rjxb}$ the $j \times b$ torque, $p_{\rm rnet}$ the charge-exchange torque, $p_{\rm rfrc}$ the rotation source friction, $p_{\rm rcmp}$ the rotation compression, $p_{\rm ntv}$ the neo-classical toroidal viscosity, $p_{\rm rpl}$ the ripple torque, $w_{\rm r}$ the thermal ion (toroidal) rotation energy, and $p_{\rm r-conv} + p_{\rm r-cond}$ the convected and conducted thermal toroidal rotation energy outflows. TRANSP assumes rigid rotation with $w_{\rm r} = 1/2 \times I_r \Omega_{tor}^2$ where I_r is the moment of inertia and Ω_{tor} is the toroidal rotation rate profile. Typically the toroidal angular momentum balance is studied instead of the power balance.

The electron particle balance equation is:

$$s_{\rm e} \equiv s_{\rm be} + s_{\rm ev} + s_{\rm ew} + s_{\rm ez} = \frac{\partial n_{\rm e}}{\partial t} + s_{\rm div} \tag{5}$$

with $s_{\rm e}$ the effective electron source rate, $s_{\rm be}$ the beam ion deposition electron source rate, $s_{\rm ev}$ the volume neutrals electron source rate, $s_{\rm ew}$ the wall neutrals electron source rate, $s_{\rm ez}$ the impurity source electron source rate, and $s_{\rm div}$ the divergence of the electron flux. In the core the last two terms on the left are negligible.

The balance equations are solved very accurately with small relative errors. across the whole TRANSP radial domain (from the plasma center to the last-closed-flux surface in the limiter discharges in TFTR, or for diverted discharges in

JET, to a flux surface close to the inboard side of the separatrix).

The thermal ion energy conduction coefficient $\chi_{\rm i}$ in engineering units is computed in TRANSP using

$$\int^{x} dV\ p_{\rm i-cond} \equiv c\ \chi_{\rm i}\ S\ n_{\rm i}\ \nabla T_i \tag{6}$$

with c the energy conversion factor, S the flux surface area and $n_{\rm i}$ the thermal ion (hydrogenic and impurity) density. The electron conduction coefficient $\chi_{\rm e}$ is defined similarly. The energy convection coefficients are defined from $\int dV\ p_{\rm i-conv}$ and $\int dV\ p_{\rm e-conv}$ using the stored thermal energies and average radial flows. The usual angular momentum transport coefficient χ_ϕ is defined using the gradient of the toroidal rotation velocity. The electron diffusivity $D_{\rm e}$ is defined using $s_{\rm div}$. We do not start the analysis with the convection and conduction terms since there are no reliable accurate models for them. In the usual TRANSP analysis mode the other terms in the balance equations are calculated from measurements and the conduction and convection terms are calculated self-consistently from those equations.

[1] J.D. Strachan, *et al.,* Phys. Review Lett. **58** (1987) 1004

[2] M. Keilhacker *et al.,* Plasma Phys. Control. Fusion (1991) **39** B1

[3] R.V. Budny, J.G. Cordey, Nucl. Fusion **56** (2016) 056002

[4] R.V.Budny, Nucl. Fusion **58** (2018) 096011, https://doi.org/10.1088/1741-4326/aaca04
There are errors in the descriptions of several plots. The temperature plotted if figure 1-e) was descried to be the measured carbon temperature $T_{\rm c}$ but instead it shows the hydrogenic ion temperature T_i which is derived in TRANSP from $T_{\rm c}$. At high values T_i is noticeably lower than $T_{\rm c}$. It more physically accurate to use both T_i and $T_{\rm c}$ with appropriate ion densities for computing $w_{\rm i}$. Figures 4-e) and 4-f) in [4] show trajectories of the central $w_{\rm i}$ versus $p_{\rm i}$. Due to a typo in the plot generators they were incorrectly labeled $w_{\rm e}$ vs time-integrated $p_{\rm e}$. Similarly figures 5-c), 5-d) and 6-a) showed the trajectories of the central $w_{\rm e}$ vs time-integrated $p_{\rm e}$. They are of $w_{\rm e}$ vs $p_{\rm e}$. The definitions of $p_{\rm i}$ and $p_{\rm e}$ used in that paper are slightly different due to the approximate energy balance equations used there.

[5] R.V.Budny, Nucl. Fusion **56** (2016) 036013

[6] R.V.Budny, Physics of Plasmas, **18** (2011) 092506
https://doi.org/10.1063/1.3626541

[7] P.R.Thomas, P.Andrew, B.Balet, D.Bartlett, J.Bull, B.deEsch, *et al.,* Phys. Review Lett. **80** 5548 (1998)

[8] Budny R.V., Bell M.G., Biglari H., Bitter M. *et al.,* Nucl. Fusion, **32** (1992) 429.

[9] M. Gorlenkova unpublished

[10] Summers H. P., "The ADAS User Manual v2.6", http://www.adas.ac.uk/manual.php

[11] Park H.P., Barnes C.W., Budny R.V., McCune D.C., Taylor G, and Zarnstorff M.C., Nucl. Fusion, **32** (1992) 1042.

[12] R.V.Budny, D.R.Ernst, T.S.Hahm, D.C.McCune, J.G.Cordey, *et al.,* Phys of Plasmas, **7** 5038 (2000)
doi: 10.1063/1.1320466

[13] R.V. Budny, M.G. Bell, D.K.M Mansfield, J.D. Strachan, S. Zweben, *et al.,* 21^{st} EPS, Montpelier, France (1994), available at http:w3.pppl.gov/~budny/PDF/Budny_EuropeanPhysicalSociety_1994.pdf

[14] S.D.Scott, D.R.Ernst, M.Murakami, H.Adler, M.G.Bell, R.Bell, R.V.Budny, *et al.,* Physica Scripta, **51** (1995) 394
doi:10.1088/0031-8949/51/3/021

[15] R.J.Hawryluk, H.Adler, P.Ailing, C.Ancher, H.Anderson, *et al.,* Phys. Review Lett. **72** 3530 (1994) http://dx.doi.org/10.1103/PhysRevLett.72.3530

[16] S.D.Scott, M.C.Zarnstorff, Cris W.Barnes, *et al.,* Physics of Plasmas, **2** (1995) 2299

[17] S.D. Scott et al IAEA 1996 (Montreal) IAEA-CN-64/A6-6 573

[18] J.G. Cordey, B. Balet, D.V. Bartlett, R.V.Budny, *et al.,* Nucl. Fusion **39** 301 (1999) doi:10.1088/0029-5515/39/3/301

[19] Joffrin E., *et al.,* "Overview of the JET preparation for Deuterium-Tritium Operation" to be published in Nuclear Fusion Special issue: overview and summary reports from the 27th Fusion Energy Conference (Ahmedabad, India, 22-27 October 2018).

discharge	mode	$< A >_{\rm hyd}$	$f_{\rm NBT}+2$	$f_{\rm Gw}$ %	$Q_{\rm DT}$	$q_{\rm DT}(0)$	$p_{\alpha e}$ MW/m^3	$\int dV p_{\alpha e}$ MW	$\int dt \int dV p_{\alpha e}$ MJ
TFTR 80539	DT supershot	2.48-2.58	2.64	53	0.28	0.8	0.300	2.5	0.7
TFTR 89402	DT supershot	2.35-2.45	2.70	25	0.29	0.45	0.053	0.36	0.45
JET 42976	DT Hot-ion H-mode	2.41-2.43	2.47	32	0.68	1.2	0.060	$\simeq$1.5	1.8
JET 42856	DT Hot-ion H-mode	2.54-2.56	2.52	34	0.68	1.1	0.042	1.6	1.6

TABLE I: *Summary of parameters for several DT discharges from TFTR and JET: The TFTR supershot 80539 with record sustained* $Q_{\rm DT}$ *and a TFTR DT supershot 89402 from the TFTR triplet and the JET Hot-Ion H-mode 42976 with record* $Q_{\rm DT}$ *and one of the alpha heating Hot-Ion H-mode discharges 42856. The values for* $< A >_{\rm hyd}$ *and* $f_{\rm NBT}+2$ *and* $f_{\rm Gw}$ *(ratio of the line-averaged* $n_{\rm e}$ *to the empirical density limit) are given at the times of maximum neutron emission. The computed values of* $< A >_{\rm hyd}$ *are non-monotonic and the values given are the ranges within the half radii. The global* $Q_{\rm DT}$*, and central values* $q_{\rm DT}$ *of the profiles are listed at the times of their peak values.* $Q_{\rm DT}$ *spiked to 0.29 in 89402 just after* $P_{\rm NB}$ *was reduced from 13.8 to 8.4MW, then decreased to 0.2 at the end of the postlude NB phase.* $q_{\rm DT}$ *is defined as the ratio of the profiles of the fusion power* $P_{\rm DT}$ *divided by the auxiliary heating power.* [3]*. Values of the central alpha-electron heating rate density and it's ratio to the central total (ion-electron* $p_{\rm ie}$*, beam-electron* $p_{\rm be}$ *and Ohmic* $p_{\rm oh}$*) heating rate densities at the times shown. The ratios increase during the discharges and listed at times within the windows of CX data and before disruptions. In equilibrium* $f_{alp} \rightarrow q_{\rm DT}/5$*. The record fusion power TFTR and JET and an ITER prediction are discussed in* [3]*.*

JET RunId 1997	TFTR RunId 1994-1995
DD 40365 Z22	DD 76649 A16
DD 41069 Z16	DD 76650 A18
TT 42840 Z25	DD 76651 A19
DT 42847 Z22	DD 76653 A12
DT 42853 Z16	DD 76654 A19
DT 42855 Z25	DT 80539 A49
DT 42856 Z22	DD 89364 A22
DT 42870 Z16	DT 89401 A36
TT 43011 Z25	DT 89405 A26
DT 42876 Z22	
DT 42982 C51	

TABLE II: *List of species, discharges used for this study, and well-validated TRANSP run ID's*

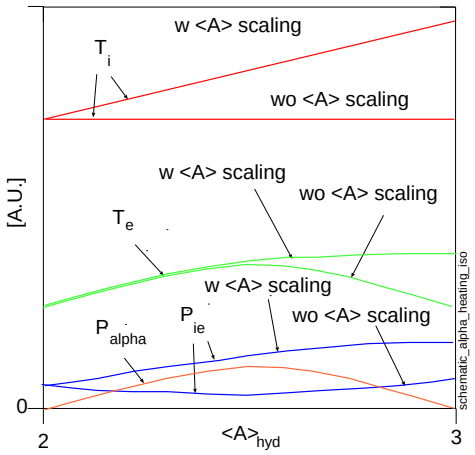

FIG. 1: (colour online) Schematic of variations of central T_i, T_e, and $p_{\rm ie} \propto (T_i - T_e)$ with the hydrogenic isotopic mass $< A >_{\rm hyd}$. With constant $n_{\rm H} + n_{\rm D} + n_{\rm T}$ the DT fusion rate is parabolic. Variations of are shown with and without isotopic mass enhancement. Measurement of T_i in comparable TT discharges could distinguish the cases.

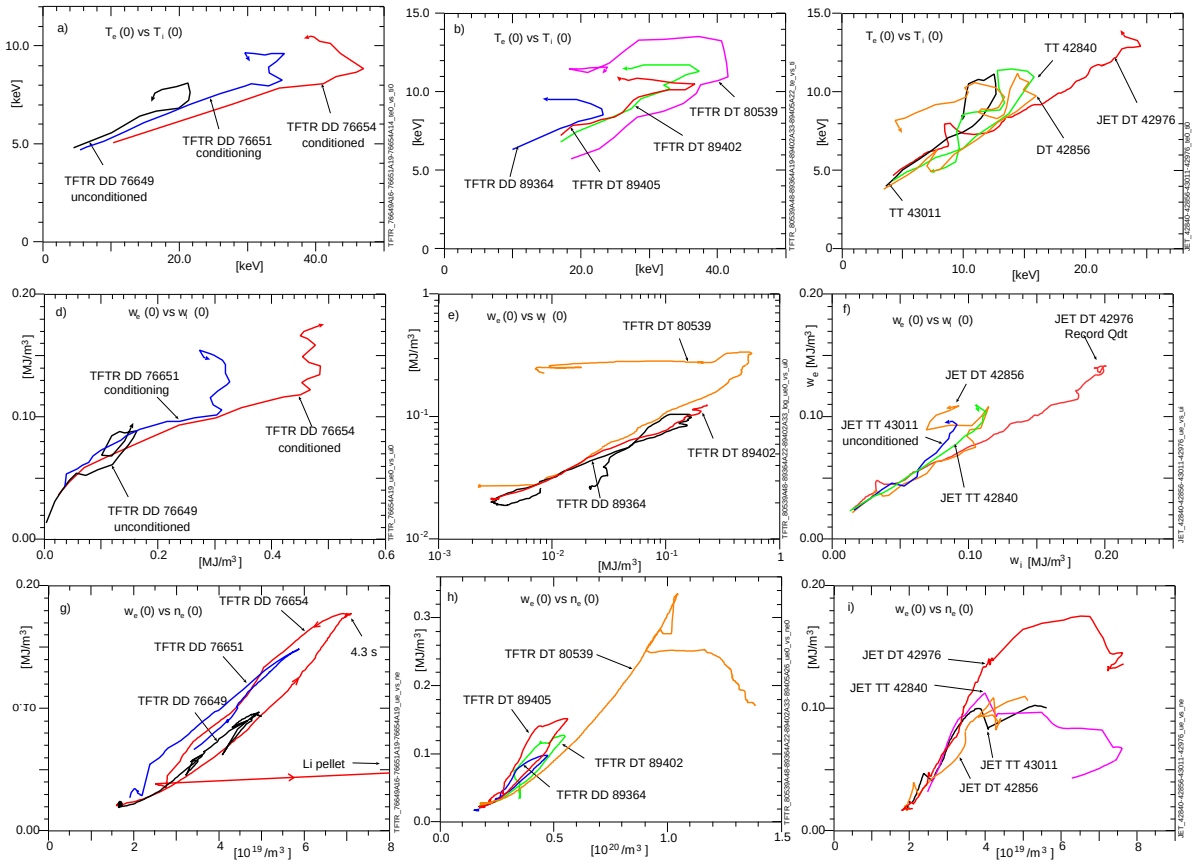

FIG. 2: (colour online) a)-c) evolutions of central values of T_e vs T_i, d)-f) central $w_{\rm e}$ vs $w_{\rm i}$ and g)-i) central $w_{\rm e}$ vs $n_{\rm e}$ from a DD wall conditioning sequence series of TFTR discharges described in [6] with increasing temperatures to supershot conditions; a set of TFTR supershots [4, 5]; and a set of JET DT and TT discharges. The start times of the trajectories are the start of NB. The end times for a)-f) are the ends of the CX data, and for g)-i) they were extended beyond the CX data time window.

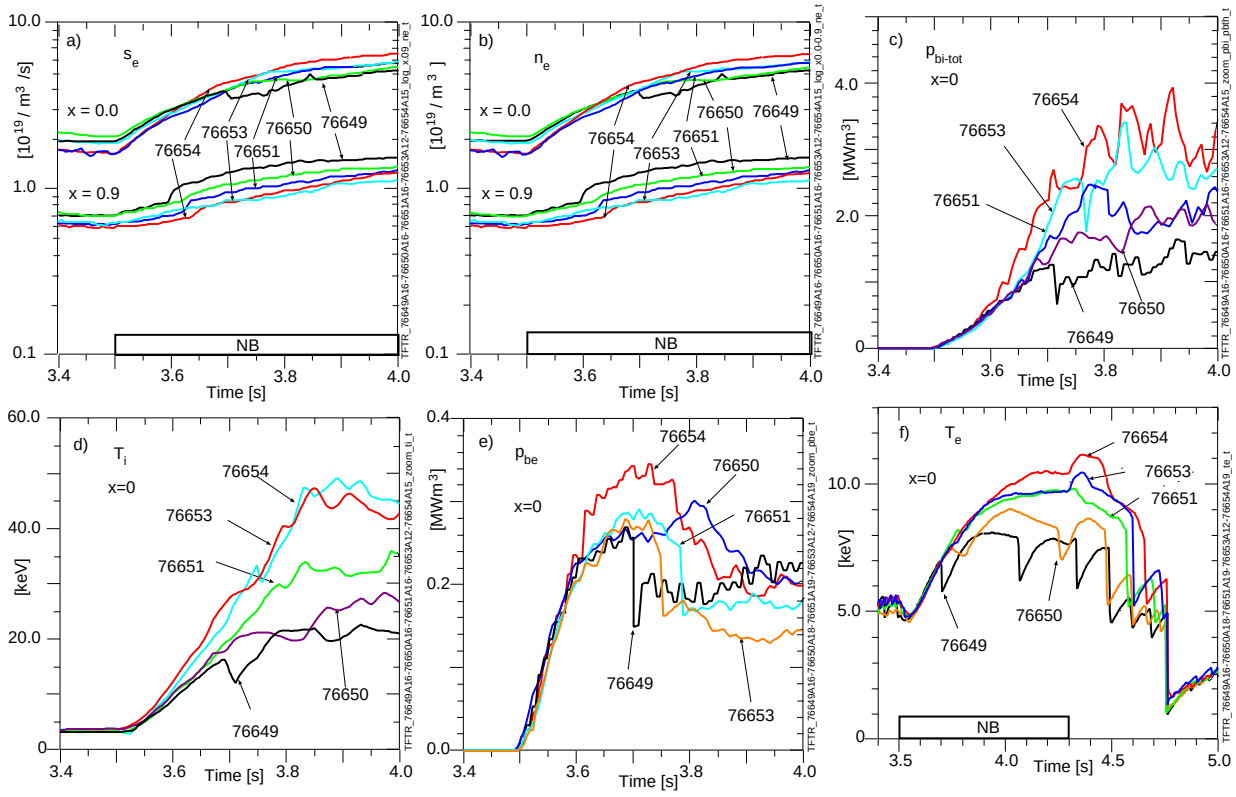

FIG. 3: (colour online) Time evolutions of parameters from the TFTR DD wall conditioning series: a) log of the electron density at the center x=0 and near the edge at x=0.9 where x is the square-root of the normalized toroidal magnetic flux (approximately the radius to minor radius ratio); b) log of the electron source rate at x=0 and at x=0.9; c) central beam ion thermal ion heating rate; d) central ion temperature; e) central electron heating rate; and f) central electron temperature. This conditioning scan is described in [6] and [4]. The NB phase, schematized in the bottom of some of the panels lasted from 3.5 to 4.3s. The abrupt decreases in T_e between 3.7 and 3.8 S are due to sawteeth. **Figure 3-b)** shows the electron source rate decreasing from discharge to discharge as wall conditions improved.

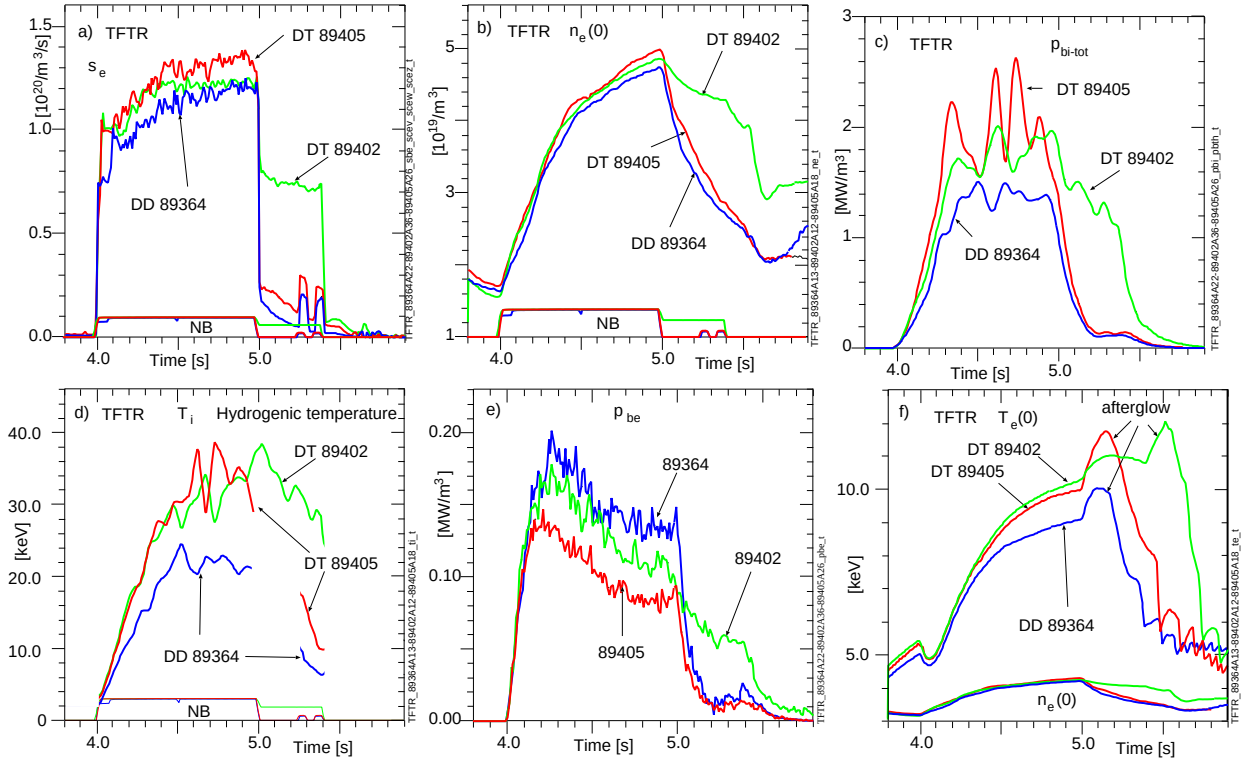

FIG. 4: (co-lour online) Evolutions of central parameters from a triplet of comparable TFTR supershots described in [4, 5]: a) NB power; b) central n_e; c) central beam ion - thermal ion heating rate; d) central ion temperature; e) central beam ion - electron heating rate; f) central electron temperature. The central electron density is schematized in the bottom of panel f).

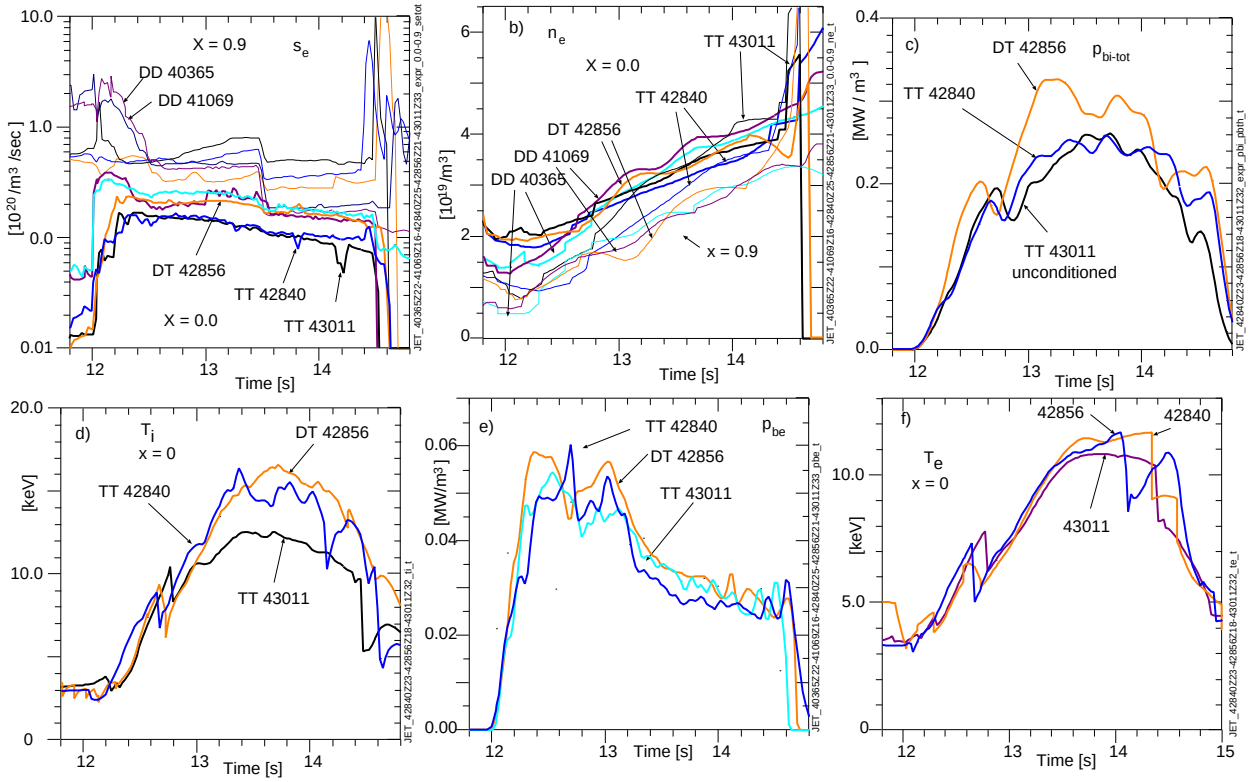

FIG. 5: (colour online) Evolutions of central parameters selected from the JET alpha heating series a) log of the electron source rate at the center x=0 and at x=0.9; b) log of the electron density at x=0 and at x=0.9; c) central beam ion - thermal ion heating rate; d) central ion temperature; e) central electron heating rate; and f) central election temperature. Two DD, one DT, and two TT discharges are shown in a) and b). The DD discharges have central electron source rate and n_e values less characteristic of the scan and thus are not closely comperable. The TT discharge 43011 had higher recycling than the others in the scan which appears to have caused the unusually low central temperatures [4, 5]. Thus this discharge should not be compared with the DT HIHM discharges.

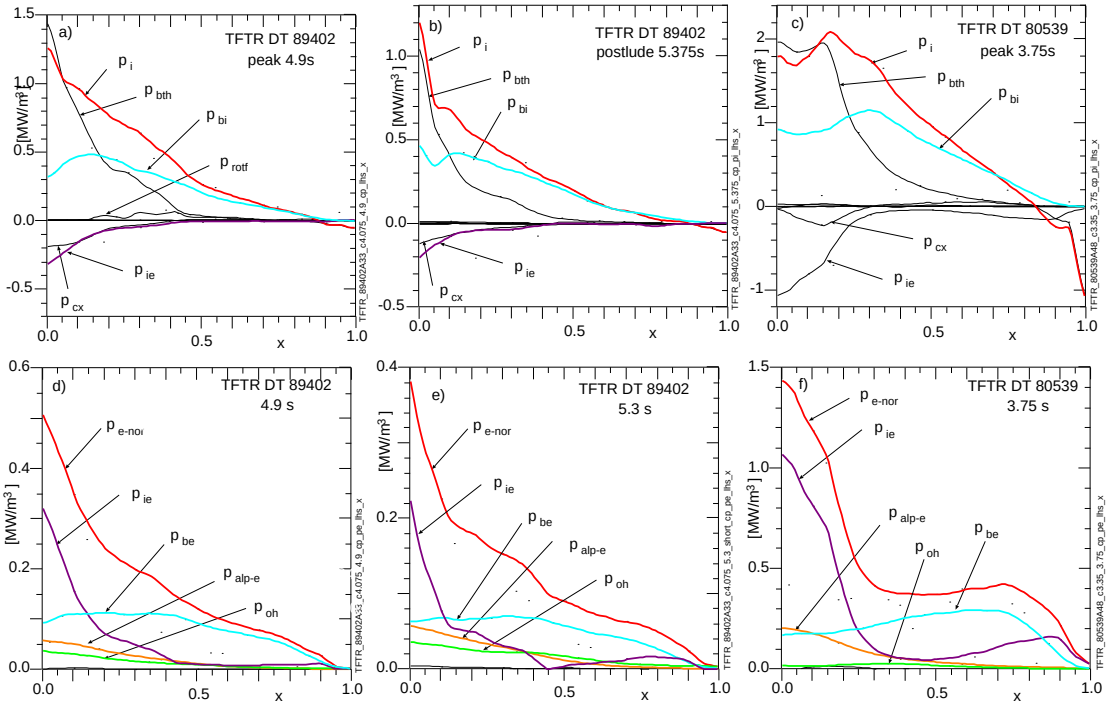

FIG. 6: (colour online) Profiles for terms in $p_{\rm i}$ and $p_{\rm e-norad} \equiv p_{\rm e} - p_{\rm rad}$ defined in equations 3 and 4 for the TFTR DT supershot 89402 from the triplet scan described in [4] and for and for the supershot 80539 with highest sustained $Q_{\rm DT}$. Two times are shown for 89042: 4.9 s near peak, and 5.3 s near the end of the postlude phase. The main NB phase for 89402 had $P_{\rm nb} = 13.8$ MW which lasted from 4 to 5s and a lower power postlude phase lasted to 5.39s. The CX data times were between 4.025 and 5.375s.

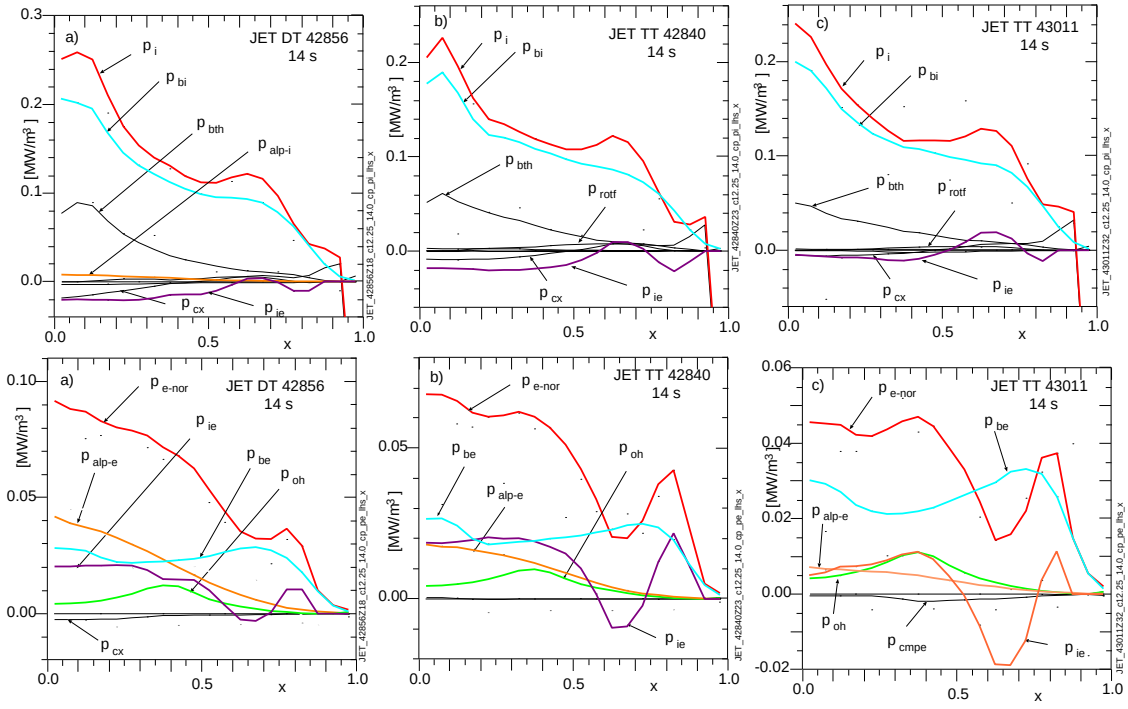

FIG. 7: Profiles of terms for $p_{\rm i}$ and $p_{\rm e-norad} \equiv p_{\rm e} - p_{\rm rad}$ defined in equations 3 and 4 for discharges form the JET alpha heating scan at 14.0s (after three of the discharges experienced their first significant sawtooth crashes) a) High performing DT 43856, b) High performing TT 42840, c) Poorly conditioned TT 43011.

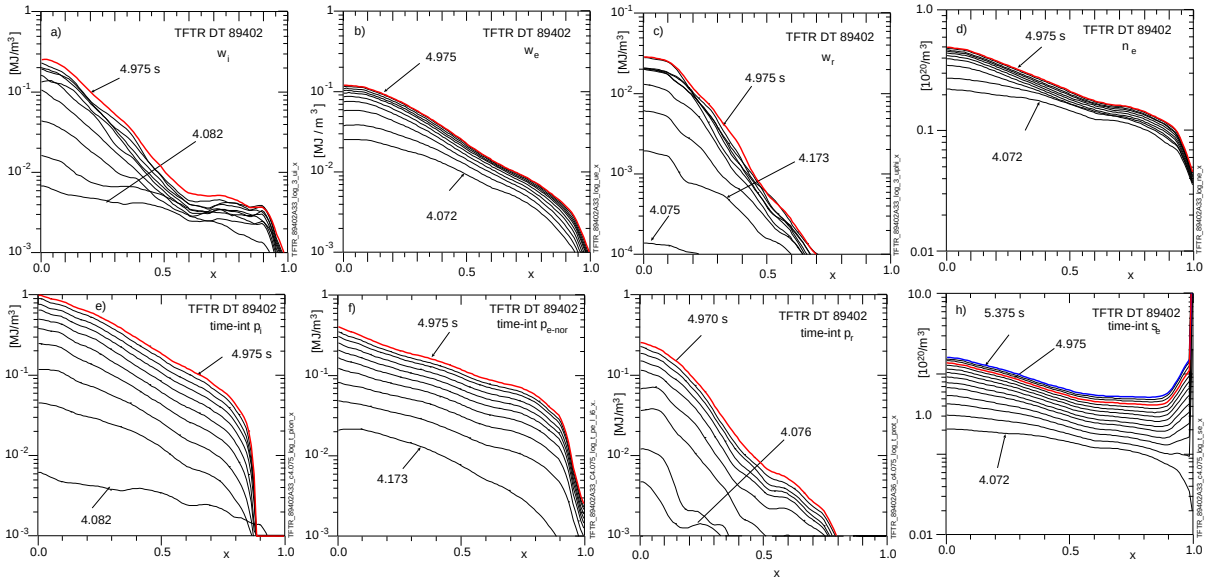

FIG. 8: (colour online) Profiles for the TFTR DT supershot 89402 shown in figure 2 at equal time increments of the densities of thermal a) ion energy, b) electron energy, c) toroidal rotation energy, and d) electron density; and of the time-integrals of the effective e) ion heating power $p_{\rm i}$, f) electron heating power $p_{\rm e-norad} \equiv p_{\rm e} - p_{\rm rad}$, g) toroidal rotation power $p_{\rm r}$, and h) electron source rate $s_{\rm e}$.

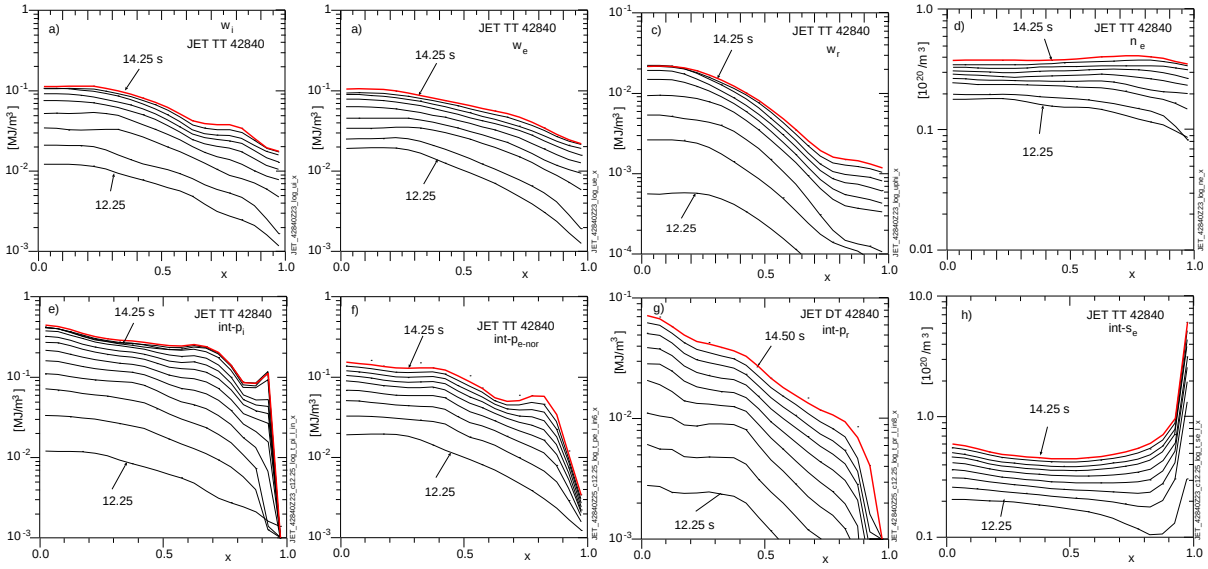

FIG. 9: Profiles for the JET HIHM TT 42840 described in [4] at equal time increments of the densities of thermal a) ion energy, b) electron energy, c) toroidal rotation energy, and d) electron density; and of the time-integrals of the effective e) electron heating power $p_{\rm e-norad} \equiv p_{\rm e} - p_{\rm rad}$, f) ions heating power $p_{\rm i}$, g) toroidal rotation power $p_{\rm r}$, and h) electron source rate $s_{\rm e}$. This HIHM was featured in [4]. The NB phase with $P_{\rm nb} = 10.6$ MW lasted from 12 to 14.7 s.

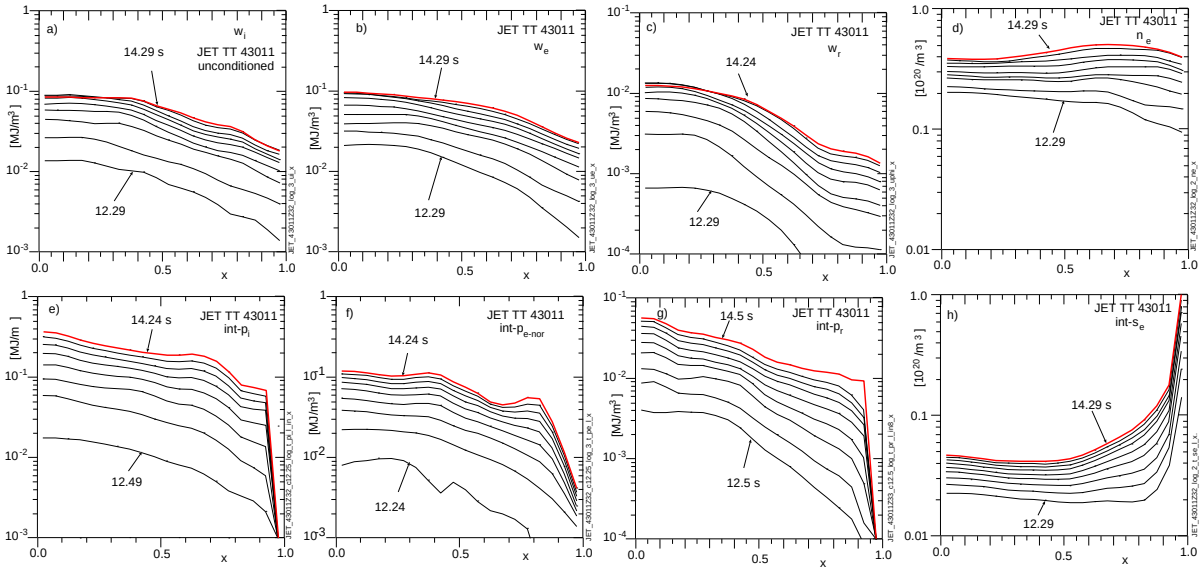

FIG. 10: Profiles for the JET poorly conditioned TT 43011 described in [4] at equal time increments of the densities of thermal a) ion energy, b) electron energy, c) toroidal rotation energy, and d) electron density; and of the time-integrals of the effective e) electron heating power $p_{\mathrm{e-norad}} \equiv p_{\mathrm{e}} - p_{\mathrm{rad}}$, f) ions heating power p_{i}, g) toroidal rotation power p_{r}, and h) electron source rate s_{e}. This HIHM was featured in [4]. The NB phase with $P_{\mathrm{nb}} = 10.6$ MW lasted from 12 to 14.5 s.

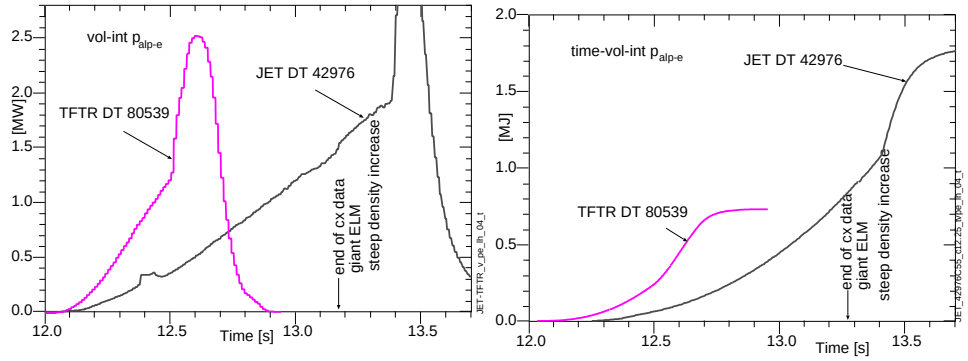

FIG. 11: Comparisons for the TFTR and JET record Q_{DT} discharges of a) $\int^t dt$, and b) $\int dV\ dt$.